Rural heat island effect of centralized residences in China: Mitigation through localized measures

Abstract

The construction movement of centralized residences in rural China may lead to energy savings and concurrently contribute to the rural heat island (RHI) effect. This effect potentially deteriorates the rural outdoor thermal environment in summer, extends periods of outdoor thermal discomfort, increases indoor temperatures, and rises energy consumption. To investigate the RHI in centralized rural residences and evaluate the effectiveness of localized heat mitigation measures, this study analyzed 22 courtyard layout patterns in a prototype centralized village in northern China through field measurements and building performance simulations. The findings reveal a heat island effect in centralized rural residences, where residential zones recorded average temperatures 1.0°C higher than those of rural boundaries. Courtyards featuring a south wing significantly alleviated outdoor thermal stress, reducing periods of extreme PET by 1.5 hours compared to those with a wall. Among the four localized heat mitigation measures examined, fabric shades stand out for their effectiveness in mitigating outdoor thermal stress, capable of reducing the courtyard's maximum T_{mrt} by 23.0°C and decreasing the duration of extreme PET by 2 hours. Photovoltaic modules not only generate energy but also alleviate outdoor thermal stress, reducing the maximum T_{mrt} by 13.0°C and lowering the daily EUI by 0.10-0.18 kWh/m², making them highly suitable for deployment in rural areas with high rates of energy poverty. The study underscores the efficacy of localized measures in mitigating the RHI effect in centralized settings, advocating for their broader application and promotion.

Keywords: rural heat island, rural centralized residences, heat mitigation measures, outdoor thermal comfort, energy consumption, courtyard layout pattern.

1. Introduction

China's implementation of the Rural Centralized Residence policy since 2004 has been instrumental in enhancing energy efficiency, yet it may also lead to the RHI effect, which can exacerbate the outdoor thermal environment during summer. Integral to rural revitalization efforts, this policy consolidates previously scattered or disorganized rural residences into centralized locations, involving either the original site or relocation (**Fig. 1**). This restructuring encompasses not just residences but also the development of essential infrastructure, including roads, energy, and water and sewage systems. According to a survey by Liu et al. on 3,685 rural households, the Rural Centralized Residence policy has been shown to reduce the energy poverty index by 14.5% through more efficient energy use [1]. However, the use of many modern facilities in newly built rural areas can also lead to a RHI effect [2, 3]. It is commonly thought that heat island issues exist only in urban areas, but rural areas also face heat island problems[4]. The transition from urban to rural environments is not a dichotomy but a gradual process [5]. From urban core areas to the urban periphery, then to rural settlements, peri-urban agriculture, and finally to natural settings, there exist different built forms, materials, and topographic features, leading to obvious differences in ground surface temperatures [6]. Additionally, temperature variations exist

within rural environments themselves. Research by Guo et al. indicates that the outdoor temperatures in town settlements and industrial areas within rural regions are significantly higher than those in farmlands and water bodies [7]. The RHI effect may degrade the outdoor thermal environment during summer, extend periods of outdoor thermal discomfort, elevate indoor temperatures, and increase energy consumption.

Fig. 1. Satellite images of centralized villages in northern China.

Common measures to mitigate the RHI effect include:

1. Optimizing outdoor space patterns influences both the absorption and reflection of solar radiation and the flow of ventilation, which are pivotal to modifying the outdoor thermal environment [8]. Studies indicate that higher height-to-width ratios in outdoor spaces usually result in lower Mean Radiant Temperatures (T_{mrt}), due to more solar radiation being absorbed in open spaces and more shade being provided in narrow spaces [9-11]. However, sometimes the height-to-width ratios of street canyons do not determine the space's T_{mrt}, because ventilation also plays a significant role [12]. For example, the layout of courtyards can alter the wind environment of outdoor spaces, thereby affecting the microclimate of these spaces [13-15].

2. Altering the surface reflectance of building materials serves as a method to adjust urban spaces' thermal dynamics. High-reflectance materials, once deemed efficacious for mitigating the UHI effects, can also alter the surrounding thermal milieu [16]. Research highlights that while increasing road reflectance can boost UCA [17], it might also escalate T_{mrt} and Physiological Equivalent Temperature (PET) in canyon-like areas [18].

3. Introducing vegetation measures can markedly refine the outdoor thermal environment. Through processes like transpiration, which curtails the dispersal of heat, and by reducing the ratio of impermeable grounds, vegetation plays a crucial role [19, 20]. The presence of trees within street and courtyard settings has been shown to substantially lower temperatures during summer in regions like the Mediterranean coast, effectively halving the increase from sunrise to midday [21].

4. Implementing shade facilities by extending architectural elements into outdoor areas can significantly affect the thermal conditions by providing shade. Evidenced by the traditional dwellings in China's Jiangnan region [22] and the semi-outdoor spaces in Singapore [23], the strategic placement of shade demonstrates a potent reduction in thermal discomfort [24]. In addition, sail-shading over urban streets is effective in reducing the surface temperatures of the street floor and building facades [25].

The effectiveness of these four methods in centralized rural settings remains undetermined due to two primary differences from urban dense areas. Firstly, rural residents are particularly sensitive to the increased costs associated with cooling measures such as air conditioning, especially among the elderly population [26]. Secondly, unlike urban canyons, centralized rural canyons include not only street spaces but also courtyards connected to the streets. In northern Chinese rural residences, courtyards are typically located on the south side of the main room, adjacent to the street, and are separated from the street by a wall or wing room [27].

Therefore, to investigate the current state of the outdoor thermal environment in centralized rural

residences, the effectiveness of local heat mitigation measures, and their impact on the corresponding indoor environment and energy consumption, this study conducted field research and experimental investigations on a typical centralized village in northern China. Initially, microclimate information of centralized rural residences and climate data from the village boundary were collected through field measurements. By comparing these two sets of data, the deterioration of the outdoor thermal environment in centralized rural residences was assessed. Subsequently, the study categorized the unique outdoor spaces of the village and simulated them using the ENVI-met software[28, 29]. An analysis of the simulation results identified the impact mechanisms of geometry scenarios and layout patterns. Following this, simulation experiments were designed to study the effectiveness of local heat mitigation measures, simulating the impact of surface reflectance, vegetation, photovoltaic modules, and fabric shade measures on the summer outdoor thermal environment, outdoor comfort, indoor thermal environment, and energy consumption. Simulation of the indoor thermal environment and energy consumption was carried out using the Ladybug Tools (LBT) software[30, 31].

Using ENVI-met to simulate the outdoor thermal environment and employing simulation results as boundary input conditions for indoor thermal environment and energy consumption simulations, this integrated approach has proven effective. Zhang et al. have shown that this methodology can not only evaluate current conditions but also quickly predict the effects of new design solutions [32].

This study presents three main innovations:

1. The RHI effect of centralized rural residences in northern China was identified by field measurements.

2. 22 types of courtyard spatial layouts in centralized residences were compared to verify the effectiveness of localized measures in mitigating the RHI effect.

3. The outdoor thermal environment, indoor thermal environment, and building energy consumption were simultaneously analyzed to identify a balanced and sustainable solution suitable for rural areas.

2. Methods

2.1 Centralized residences: a case study of Hangtou village

2.1.1. Site and layout pattern

Hangtou Village located in Lingyang Town, Ju County, Shandong Province, China, approximately 2 kilometers southeast of Ju County's city center (118.86’E, 35.54’N). The village was renovated in its original location 11 years ago. After renovation, Hangtou Village maintained its compact form, featuring a grid of orthogonal streets, streets of uniform width, and residences of consistent size. We used a DJI-Inspire-2 drone to take aerial photography of the centralized residences and their surroundings, generating a 3D point cloud model (**Fig. 2**(a)), which reveals that Hangtou Village is divided into northern and southern clusters, comprising three geometry scenarios.

The northern cluster includes Geometry Scenario 1 (GEO1) and Geometry Scenario 2 (GEO2), both scenarios sharing common spatial proportions but differing in the variation of surface textures (**Fig. 2**(b)). Based on three different wing room layout configurations within the courtyard, the northern cluster has a total of six layout patterns (G1-1 to G2-3) (**Fig. 2**(c)). The south side cluster has only one spatial scale of geometry 3 (GEO3), and unlike the north side residences, the south side residences have five widths of 6 m, 9 m, 12 m, 15 m, and 18 m in the E-W direction, and the main room is mainly a one-story sloped-roofed house with a height of 6 m. The layout of courtyards in the south side cluster, with the east side wing room being the most common, are 15 actual layout patterns (G3-1 to G3-15).

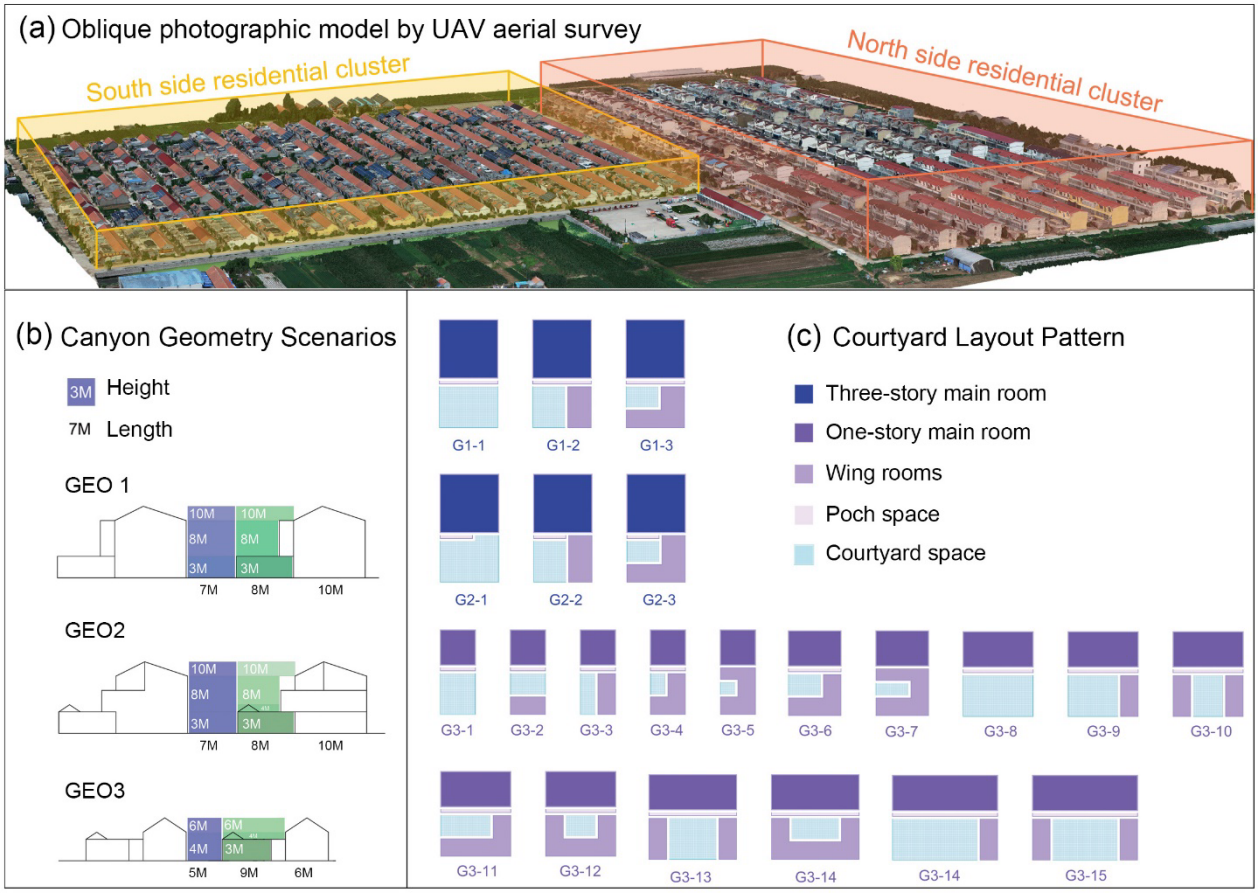

Fig. 2. Canyon geometry scenarios and courtyard layout patterns of rural centralized residences.

2.1.2. Localized heat mitigation measures

Based on the survey, Hangtou Village has eight local heat mitigation measures (**Fig. 3**). First are three types of building surface material reflectance, ranked from low to high: gray cement walls with the reflectance ratio of 0.3, yellow painted walls with the reflectance ratio of 0.5, and white painted walls with the reflectance ratio of 0.7. Next, there are three types of vegetation measures: minimal vegetation, featuring small trees on the side of the street closest to the courtyard; moderate vegetation, which adds a large tree to the minimal vegetation within the courtyard; and extensive vegetation, which builds upon minimal vegetation by incorporating numerous small trees within the courtyard. The fabric shading is a net prepared from nylon, which is black with apertures, effectively blocking direct sunlight and allowing air to circulate freely. Lastly, solar panels, installed on the roofs of wing rooms and main rooms, convert solar energy into electricity and at the same time create a shading effect on the canyon space. These solar panels are tilted at 45° and are slightly larger than the size of the south side of the sloped roofs. In addition, there are also single-story red tile roofs, single-glazed windows, light-colored concrete floors, and planted ground surfaces that are consistent in each house, and these materials, although they have an impact on the outdoor thermal environment, do not become a variable scenario for the study but rather exist as a fixed background.

Fig. 3. Localized heat mitigation measures.

2.2. Microclimate data measurement

Hangtou Village is in a warm temperate monsoon continental climate zone with distinct seasons and abundant rainfall. The average annual air temperature (T_a) is 13.6°C, with the highest recorded T_a at 37.1°C in July and the lowest at -16.8°C in January. On our field measurement day, July 31, 2023, data from the Juxian weather station (NO.54936JUXIAN) indicated a maximum T_a of 30.4°C, an average T_a of 27.5°C, relative humidity (RH) of 96%, and wind speed of 3.1m/s. However, due to the distance from the weather station to our actual measurement site, more detailed microclimate data was required. Thus, a PC-6 type micro weather station was deployed at a community activity square on the edge of the residential area (**Fig. 4**(e)). This station recorded a maximum T_a of 31.4°C, an average T_a of 29.2°C, RH of 80.8%, a wind speed of 2.8m/s, a maximum direct solar radiation of 502 W/m², and a maximum total radiation of 1026W/m².

Fig. 4. Field measurement locations, scenarios, and instruments.

In the field measurement section, we selected three typical residences for assessing the outdoor thermal environment and indoor T_o (**Fig. 4**(a)). Residence No.1 (R-1) belongs to GEO 1, G1-2 pattern, featuring high reflectance white paint, and employed extensive vegetation and fabric shade measures. Residence No.2 (R-2), situated in the southern cluster, corresponds to GEO 2, G3-12 pattern with white paint, but using minimal vegetation and photovoltaic module measures. Additionally, R-2's courtyard lacks greenery, has cement flooring, and features an operable glass roof which was closed during measurement. Residence No.3 (R-3), falls under GEO 3, G3-13 pattern, with white paint and a moderate vegetation measure, having a completely open courtyard on top. The micro weather station was placed at the intersection of the northern and southern clusters, which provides an approximately 3000 m^2 open space conducive for capturing accurate climate data. The parameters of the measuring instrument are detailed in **Table A. 1**.

To evaluate the outdoor thermal environment, we utilized measured T_a, globe temperature, and wind speed to calculate the mean radiant temperature (T_{mrt}) in street and courtyard spaces. The calculation formula, according to ASHRAE (2001), is as follows:

$$T_{mrt} = \left[\left(T_g + 273.15\right)^4 + \frac{1.1\times10^8 V_a^{0.6}}{\varepsilon \times D^{0.4}} \times \left(T_g - T_a\right)\right]^{0.25} - 273.15 \quad (1)$$

Where:

T_{mrt} is the mean radiant temperature in degree Celsius,

T_g is the globe temperature in degree Celsius,

T_a is the air temperature in degree Celsius,

V_a is the air velocity in meter per second,

D is the globe diameter in meter, and

ε is the globe emissivity.

We calculated the PET values for the courtyard and the street using Rayman software [33], in which the T_a

and wind velocity were obtained from field measurements, the T_{mrt} was obtained by calculating formula 1, and the Sky View Factor (SVF) was obtained by calculating the fisheye photographs and Rayman software.

2.3. Models and simulation

Eight ENVI-met models were developed to simulate the outdoor thermal environment, corresponding to the heat mitigation measures mentioned in **Fig. 3**. To control experimental variables, the models for minimal vegetation, moderate vegetation, extensive vegetation, photovoltaic modules, and fabric shade, all walls were of high solar reflectance. The settings for material parameters involved in other scenarios are listed in **Table B. 1**. The ENVI-met software configuration parameters can be found in **Table B. 2**.

In the LBT modeling process, the environmental data were kept as consistent as possible with ENVI-met. Meteorological information was based on data from the EnergyPlus weather website's NO.54936JUXIAN station and outputs from ENVI-met simulations were adjusted using MATLAB software for variables such as Dry Bulb Temperature (°C), Dew Point Temperature (°C), Relative Humidity (%), Direct Normal Radiation (Wh/m²), Diffuse Horizontal Radiation (Wh/m²), Wind Direction (degrees), and Wind Speed (m/s). The construction information of the residential models was kept consistent with ENVI-met, and for materials or physical properties not present in LBT, new elements were created to ensure the physical properties (**Fig.B. 2**). Detailed information about the models, including adjacency relationships between rooms, room usage types, sizes and materials of interior doors and windows, shading materials, and the detailed settings of the four heat mitigation measures, can be found in the **Fig.B. 1** and **Fig.B. 3**.

3. Results

3.1. Field measurement

When compared with the micro weather station data, the measured outdoor T_a in the three residences is delayed and the value is higher, which indicates that there is a heat island effect in the rural settlement. The courtyard of R-1 and R-3 and the streets of R-1, R-2, and R-3 experienced a gradual increase in T_a from less than 29.0°C at 10:00 a.m. to a peak of about 31.0°C by 2:00 p.m., followed by a decrease to the lowest temperature of about 28.0°C by 6:00 p.m. The micro weather station recorded the peak T_a at noon, two hours earlier than the residences, with the highest temperature recorded at 31.0°C, which is 1.0°C lower than that of the residences (**Fig. 5**(a)). The T_a at the R-2 courtyard measurement point was significantly higher than at other points, with the highest value appearing one hour later, which can be attributed to the courtyard's roof being a closed glass skylight, leading to poor air circulation within the courtyard.

The trends in RH closely mirror those of T_a changes. This is because, in the absence of additional moisture or specific local climate influences, the absolute humidity in the air remained constant throughout the day (**Fig. 5**(b)).

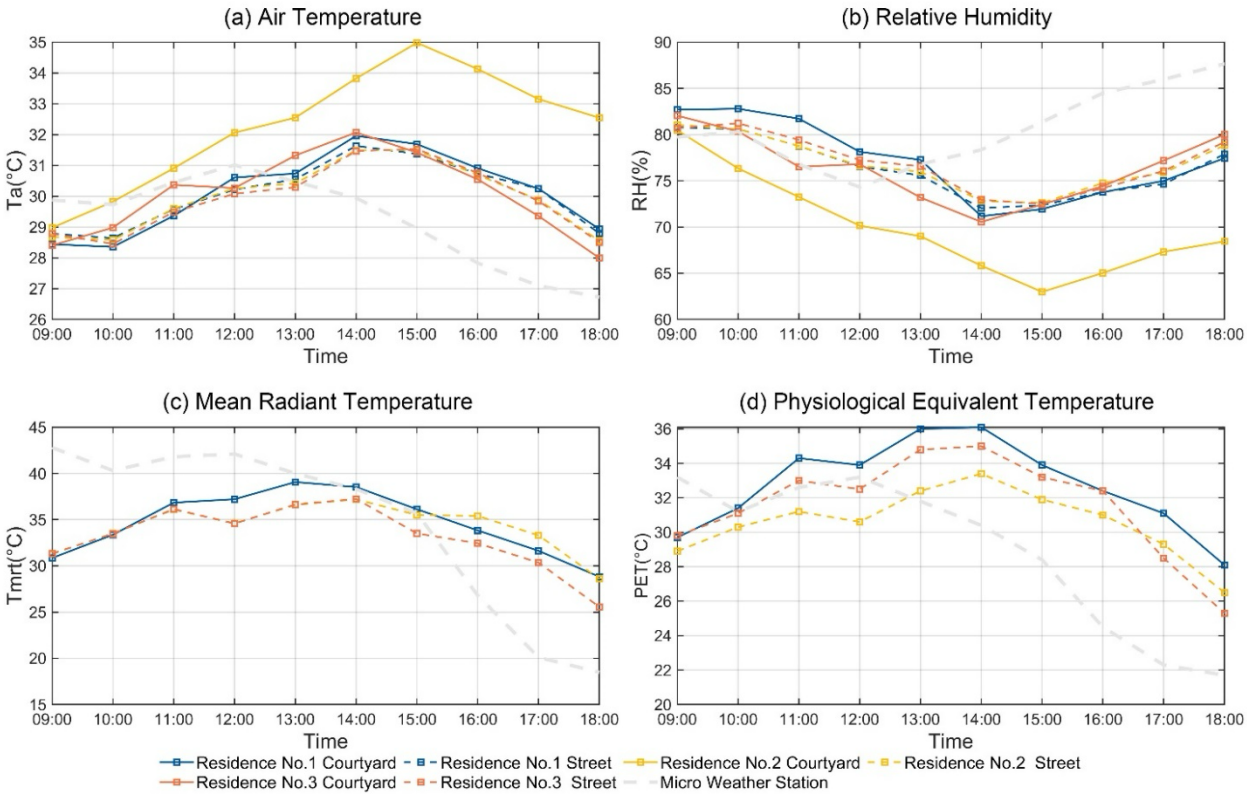

Fig. 5. Comparing the measured data from three residences and the micro weather station.

The T_{mrt} results show that the absorption of solar radiation by centralized residences was delayed. The T_{mrt} data of the three sites were lower than that of the micro weather station data until 2:00 p.m., and the T_{mrt} of the three sites was around 31°C at 9:00 a.m. and reached a maximum of around 36°C at 1:00 p.m. to 2:00 p.m. The T_{mrt} data of the micro weather station was in the range of 40°C to 45°C until 13:00, and then exceeded the data at 3:00 p.m. (**Fig. 5**(c)). Due to the damage of some of the Black Sphere instruments, T_{mrt} and PET data were calculated and compared with the micro weather station data only for the R-1 courtyard and the streets of R-2/R-3.

The PET calculations show that the three residences were in the thermal discomfort range for most of the day, but were consistently below the extreme heat stress range. The PET maxima were around 36°C for the R1 yard, and around 34°C and 35°C for the R2, and R-3 streets, respectively. The PET calculated from the micro weather station data peaked at 33°C at 12:00 a.m., 1-2 hours earlier than the peaks for the three residences. (**Fig. 5**(d))

The observed phenomena could be attributed to the differing geometry factors of the three typical courtyards or the effects of local heat mitigation measures, such as the extensive vegetation in R-1, white fabric shade overhead, solar panels forming shades on the south side of R-2, and moderate vegetation measure of R-3. However, the specific impact of geometry factors and local heat mitigation measures on reducing the RHI effect of centralized residences, as well as their effectiveness and magnitude, requires further experimentation with controlled variables.

3.2. Model validation

The validation results for the ENVI-met and LBT models indicate high accuracy (**Fig. 6**). The correlation coefficient (R^2) for the outdoor T_a simulated by the ENVI-met model is 0.99 (**Fig. 6**(a)), for outdoor RH is 0.98

(**Fig. 6**(b)), and for outdoor T_{mrt} is 0.97 (**Fig. 6** (c)). The indoor T_a simulated by the LBT model shows an R^2 of 0.95 (**Fig. 6**(d)).

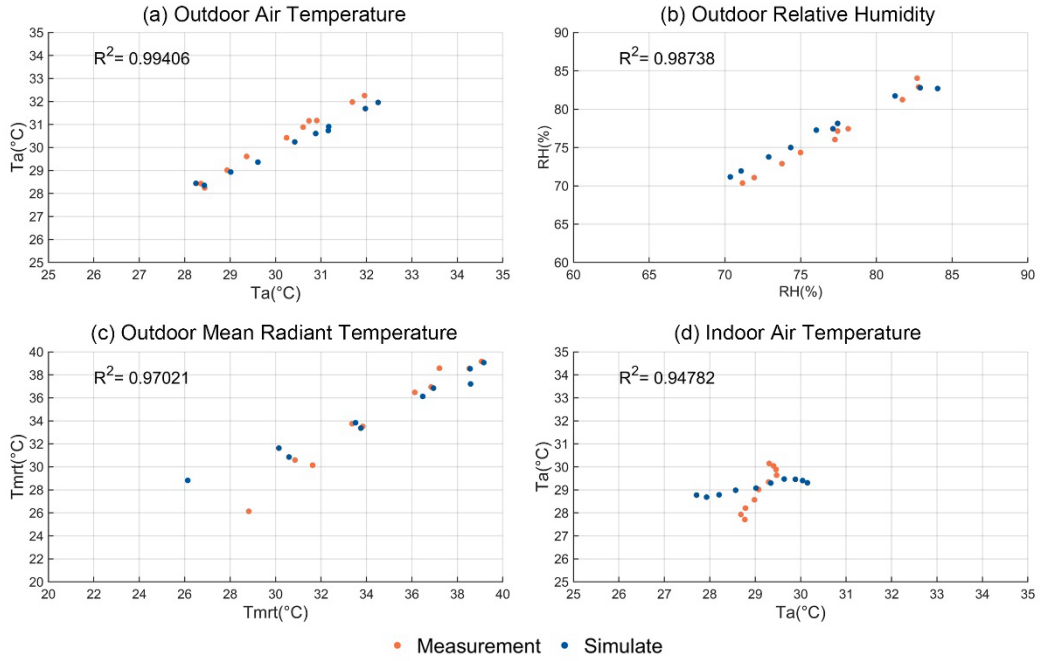

Fig. 6. Correlation analysis between measured and simulated data.

3.3. Outdoor climate analysis of the centralized residence

3.3.1 Geometry and layout pattern

This paper uses T_{mrt} and PET indexes to assess the changes in the outdoor thermal environment and thermal comfort, which have been used in many studies of outdoor microclimate [34-36]. The simulation results show that the T_{mrt} values for the courtyards with a south wing are significantly lower than those for the courtyards with a south wall, but the T_{mrt} for the street space is not affected. The maximum T_{mrt} in courtyard G1-3 is 60.7°C, which is lower than the 65.5°C observed in courtyards G1-1 and G1-2. Similarly, the maximum T_{mrt} in courtyard G3-4 is 64.3°C, lower than the 71.1°C in courtyard G3-3. The same trend is observed between G3-14 and G3-13, as well as G3-11 and G3-9. The T_{mrt} data for street spaces from G1-1 to G1-6 and from G3-1 to G3-16 are essentially identical (**Fig. 7**).

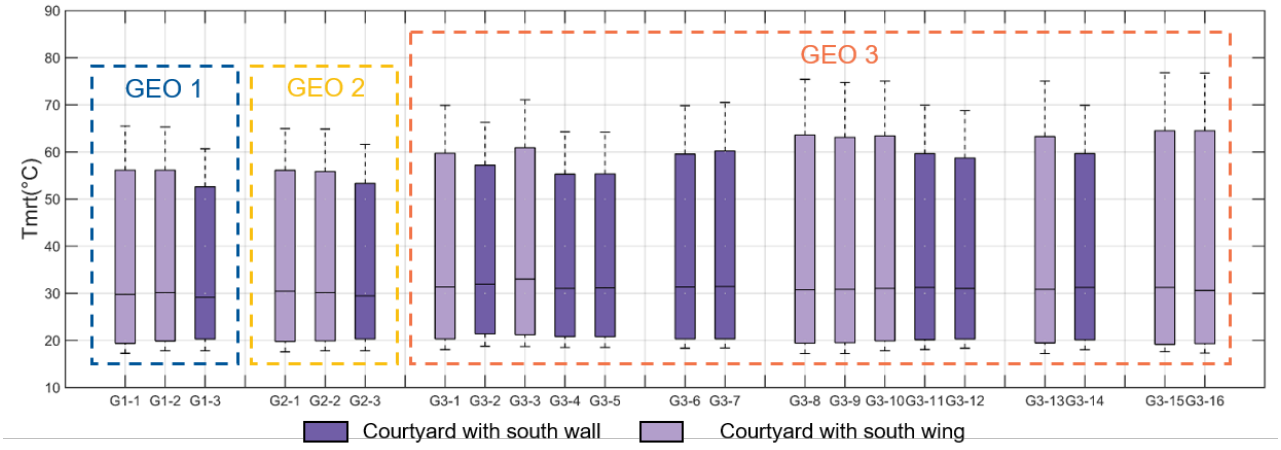

Fig. 7. T_{mrt} in courtyards of residences with different layouts under high solar reflectance scenario.

The height-to-width ratio of outdoor spaces plays a primary role in the variation of T_{mrt} within the space. The higher the ratio, the lower the T_{mrt} values within the space. The T_{mrt} values for courtyards and streets under GEO 1 and GEO 2 scenarios are almost always lower than those under the GEO 3 scenario. Additionally, the data for G1-1 and G1-4, G1-2 and G1-5, G1-3 and G1-6 are almost the same, which indicates that the wall bumps in the space have almost no effect on T_{mrt}.

The simulation results show that the T_{mrt} values for the street space in the same geometry scenario are basically the same. Comparing the heterogeneity of the T_{mrt} of the courtyard space in the same street indicates that ventilation may play a decisive role in the T_{mrt} of the street space.

Through the above analyses, we learned that the differences in courtyard T_{mrt} are mainly due to the varying aspect ratios between GEO1 and GEO3, as well as the layout configurations of courtyards with a south wing or south wall. To compare the impacts of various heat mitigation measures more efficiently and clearly, we selected two pairs of residences, G1-2 and G1-3, G3-10 and G3-12, containing geometry and layout factors for the result analysis instead of analyzing all the residences simulation results. (**Fig. 8**)

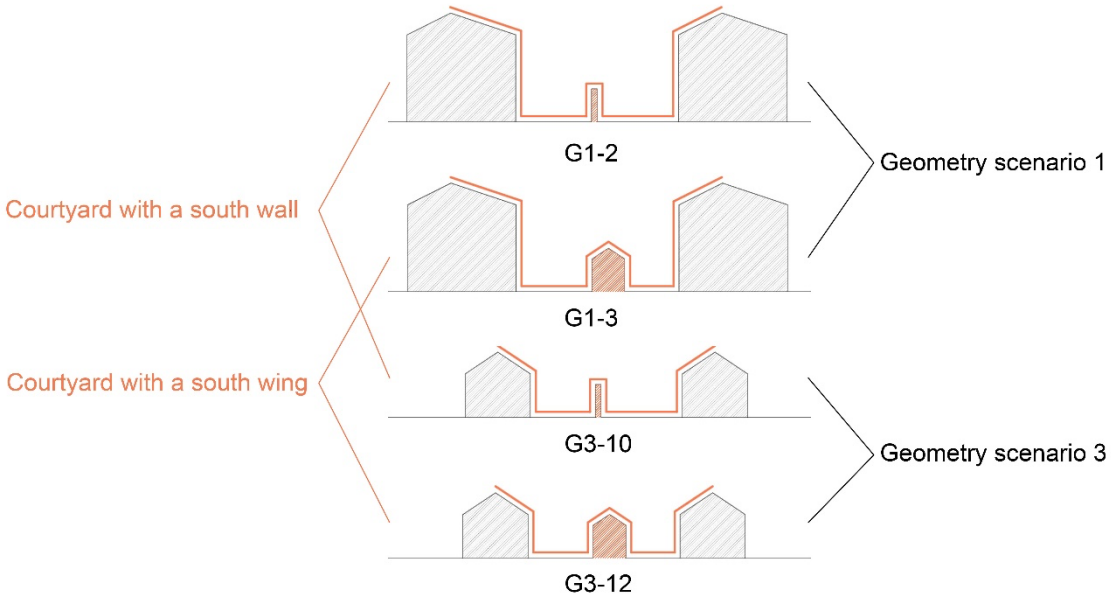

Fig. 8. Diagram of courtyard with a south wing or a south wall in different rural canyon geometry scenarios.

3.3.2 Solar reflectance ratio of building surface materials

The simulation results show that the outdoor T_{mrt} of the four residences increases with increasing the solar reflectance ratio of the building surface material, but the effect is very weak (**Fig. 9**). The lowest T_{mrt} in each residence's courtyard is around 18°C. For G1-2, the highest T_{mrt} increases from 61.9°C to 65.3°C; for G1-3, it rises from 56.9°C to 60.7°C; for G3-10, from 71.0°C to 75.1°C; and for G3-12, from 65.3°C to 70.0°C (**Fig. 9**(a)). The size relationship between the four residences also shows that altering the building surface solar reflectance ratio has no conflict with the impact of geometry and layout on the outdoor thermal environment (**Fig. 9**(b)).

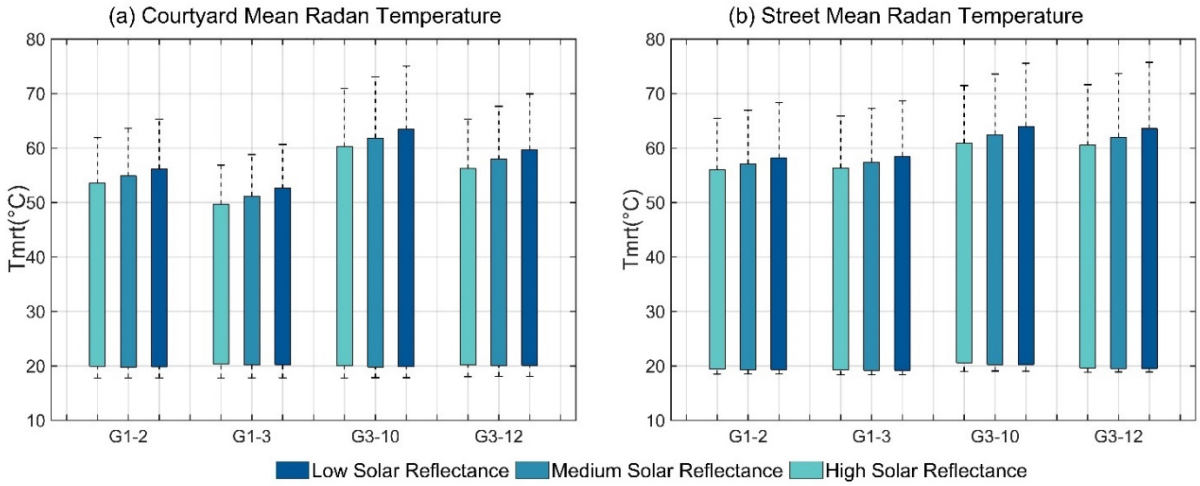

Fig. 9. T_{mrt} of 4 Residences under different solar reflectance scenarios.

3.3.3 Vegetation measures

Simulation results showed clear impact of vegetation on reducing outdoor T_{mrt}. With the increase of greening area, the T_{mrt} values in the residential courtyard are effectively reduced. The highest T_{mrt} value of G1-2 in the courtyard is 63.3°C in the minimal vegetation measure, which is a decrease of 2.0°C compared to the none-measured model, and the highest T_{mrt} decreases by 10.1°C in moderate vegetation and 19.3°C in extensive vegetation (**Fig. 10**).

The effect of the layout factor is much weaker when using the extensive vegetation measures, but the effect of geometry factor is consistently more pronounced. G1-3, sharing the same GEO 1 as G1-2, sees its courtyard T_{mrt} values decrease by an additional 2.7°C under minimal and moderate vegetation measures compared to G1-2. However, with the adoption of extensive vegetation measures, the T_{mrt} values of G1-2 were the same as those for G1-3 courtyards. In contrast, under all three vegetation measure scenarios, the courtyard T_{mrt} values of G3-10 are consistently higher than those of G1-2 in corresponding conditions.

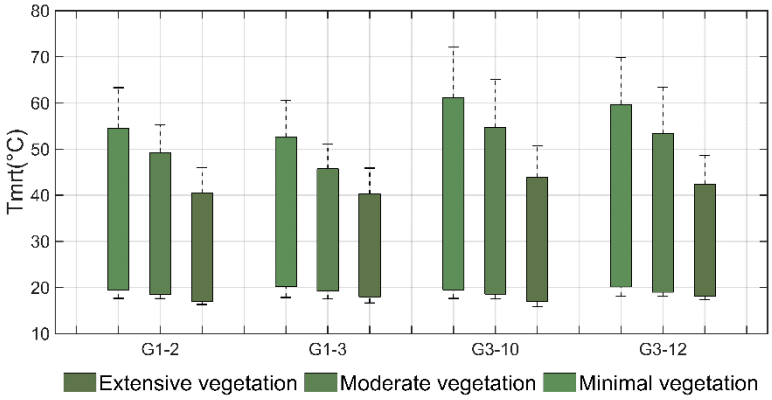

Fig. 10. T_{mrt} in courtyards of residences under different vegetation measures scenario.

3.3.4 Comparison of four heat mitigation measures

Based on previous results, we know that measures capable of reducing courtyard T_{mrt} include increasing the space's height-to-width ratio, adopting a courtyard with a south wing layout pattern, using low solar reflectance materials, and implementing extensive vegetation measures. Besides these strategies, solar photovoltaic module measures and fabric shade measures are widely used as heat mitigation strategies. To comprehensively compare the effectiveness of these measures, we use high solar reflectance as the base model to summarize the maximum T_{mrt} of these measures in the outdoor spaces of the four residences.

The comprehensive results show that for reducing spatial T_{mrt}, extensive vegetation measures and fabric shade measures are the most effective strategies. Photovoltaic module measures are effective in GEO 2, while low solar reflectance measures have the least impact. Extensive vegetation measures could reduce the maximum T_{mrt} values in courtyards of G1-2 and G1-3 by 14.8-19.4°C, and for G3-10 and G3-12, by 19.1-24.4°C, respectively. Fabric shade measures have a slightly lower cooling effect than extensive vegetation measures, reducing T_{mrt} by about 2.0°C less. Photovoltaic module measures have no effect on G1-2 and G1-3, but can reduce T_{mrt} by 10.9-13.0°C in the courtyards of G3-10 and G3-12. Low solar reflectance measures only manage to reduce T_{mrt} by about 3.0°C across all spaces. Lastly, all heat mitigation measures have a minimal effect on reducing max T_{mrt} in street spaces (**Fig. 11**).

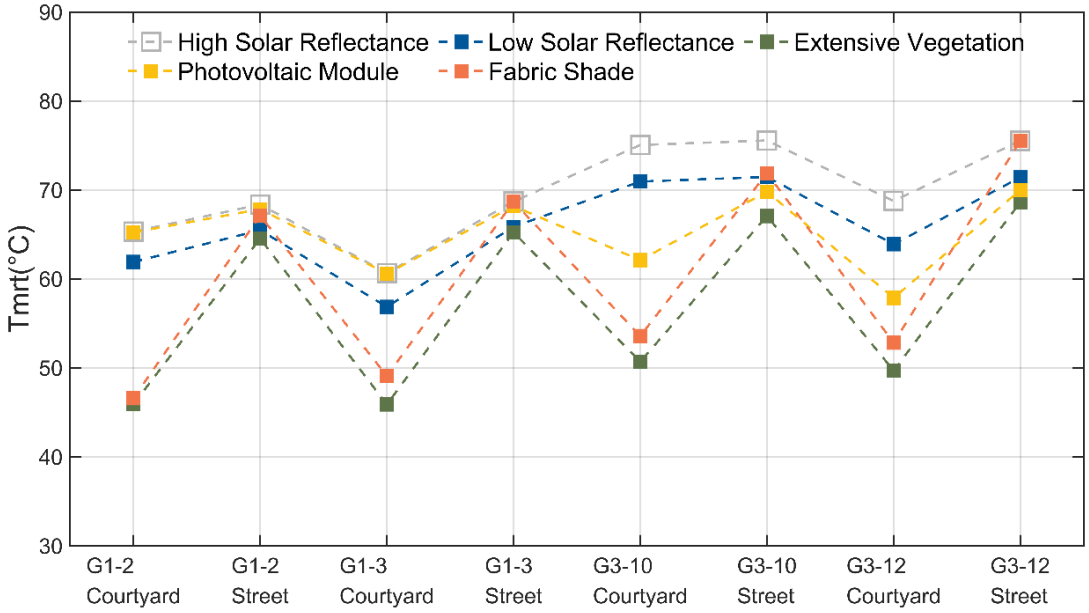

Fig. 11. Maximum T_{mrt} of courtyard and street space under localized heat mitigation measures.

PET simulation results reveal that the four localized heat mitigation measures' effectiveness in reducing the duration of extreme heat stress is consistent with their ability to lower courtyard T_{mrt} maximum values. Extensive vegetation measures can reduce the duration of extreme heat stress by approximately 3 hours, fabric shade measures by 1.5 to 2 hours, and photovoltaic module measures by about half an hour, while the effect of low solar reflectance measures is very weak. Similarly, all measures have no effect on reducing the duration of extreme heat stress for street PET. Fabric shade measures may even slightly increase PET in the street spaces of G3-10 and G3-12 (**Fig. 12**).

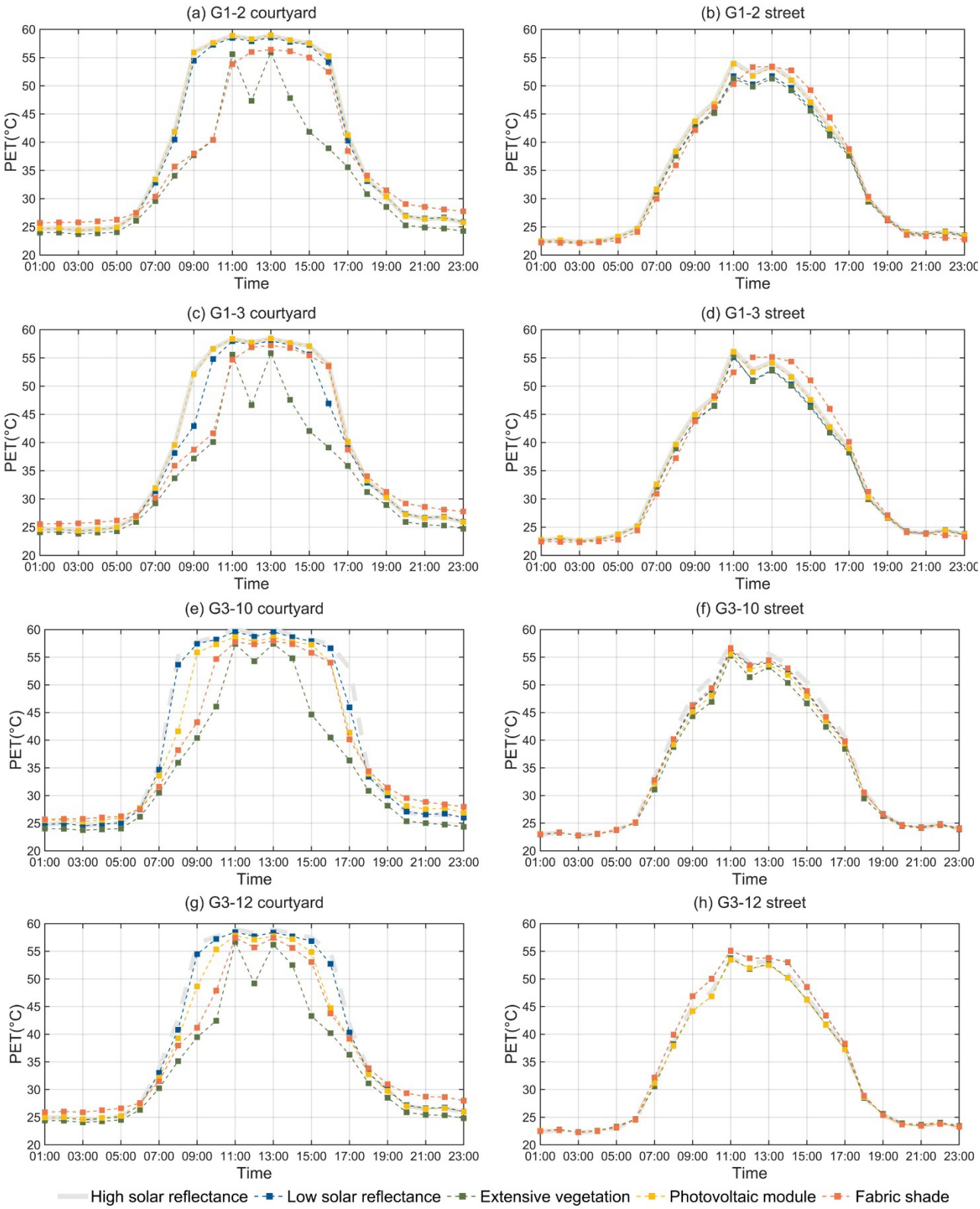

Fig. 12. Impact of heat mitigation measures on the temporal distribution of PET

3.4. Indoor environment and building energy consumption

Low solar reflectance measures result in a slight increase in indoor T_o, which contrasts with the trend observed outdoors. The simulation results for the living rooms on the first floor of the four residences show that

low reflectance measures can cause T_o to rise by 0.1-0.2°C (**Fig. 13**). Compared to the base model, the other three local heat mitigation measures all contribute to a reduction in indoor T_o. Fabric shade measures are the most effective, potentially lowering T_o by up to 6.5°C. Extensive vegetation measures can reduce T_o by up to 4.0°C, and photovoltaic module measures can also decrease T_o by up to 4.0°C, though their overall impact is not as significant as that of extensive vegetation measures.

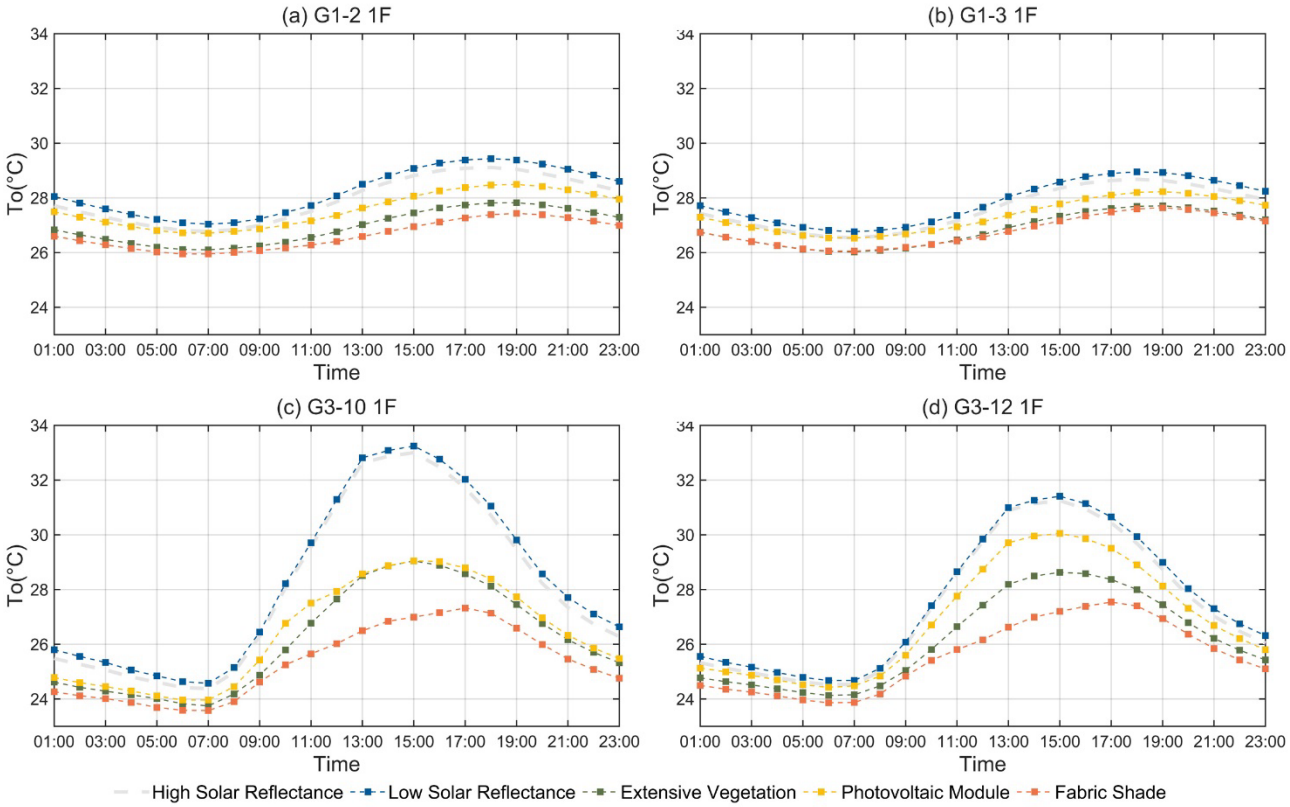

Fig. 13. Impact of local heat mitigation measures on the temporal distribution of indoor T_o.

The LBT simulation results indicate that photovoltaic module measures, due to their ability to generate electricity, result in the lowest overall energy consumption. With photovoltaic module measures, residences G1-2 and G1-3 can generate 29.4 kWh of electricity per day, and G3-10 and G3-12 can generate 38.5 kWh per day (**Table 1**), leading to a significant reduction in the daily energy usage intensity (EUI) for these homes, by more than half in some cases (**Fig. 14**). The effectiveness of the other measures is consistent with the effectiveness of the indoor T_o reduction (as the main energy consumption is the cooling demand). Using the fabric shade measure, the energy consumption of the four residences is essentially flat, with an EUI of 0.35 kWh/m^2, a reduction of 0.04-0.17 kWh/m^2 compared to the base model, while the extensive vegetation measure reduces it by 0.03-0.13 kWh/m^2, and the low solar reflectance measure increases 0.01-0.04 kWh/m^2.

Table 1.
Daily electricity generated by photovoltaic module measure.

	G1-2	**G1-3**	**G3-10**	**G3-12**
Wing room solar panels (kWh)			17.354158	17.332781
Main room solar panels (kWh)	29.35088	29.31529	21.115509	21.08994
Total electricity (kWh)	29.35088	29.31529	38.46967	38.42272

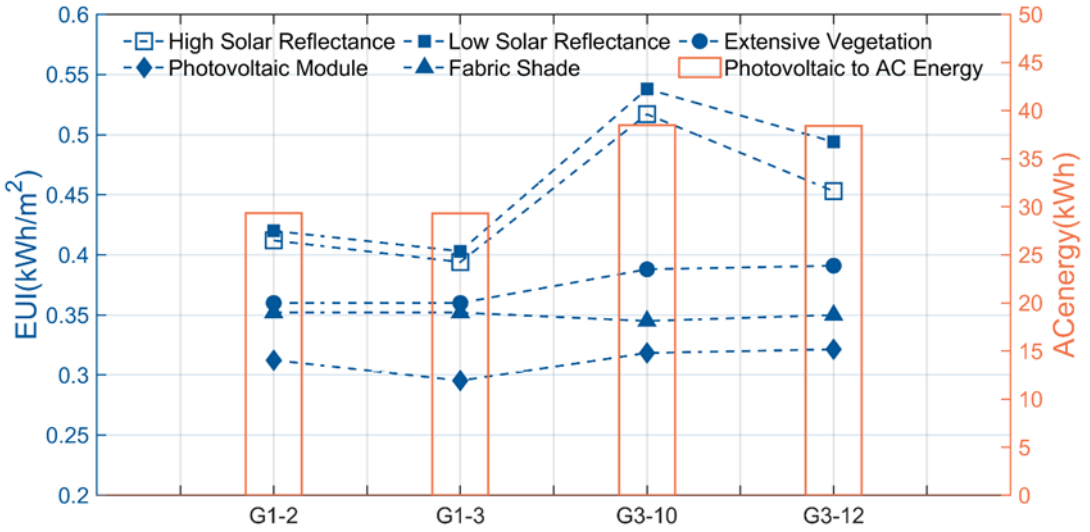

Fig. 14. Simulate day EUI under local heat mitigation measures (left) and photovoltaic module AC energy generated (right).

4. Discussion

4.1 Analysis and recommendation of localized heat mitigation measures

After comparing the effects of various heat mitigation measures on outdoor thermal comfort, indoor T_o, and energy consumption across different scenarios, it indicated that no single measure is perfect in reducing the RHI effect. A quantitative comparison across these three dimensions is needed to assess the comprehensive performance of each measure. Since the difference in building energy consumption during summer is mainly due to variations in cooling energy demand, there is a correlation between indoor T_o and EUI. Considering the poor readability of three-dimensional scatter plots, a two-dimensional scatter plots of courtyard average PET and EUI are used to represent the performance of each measure in different directions (**Fig. 15**).

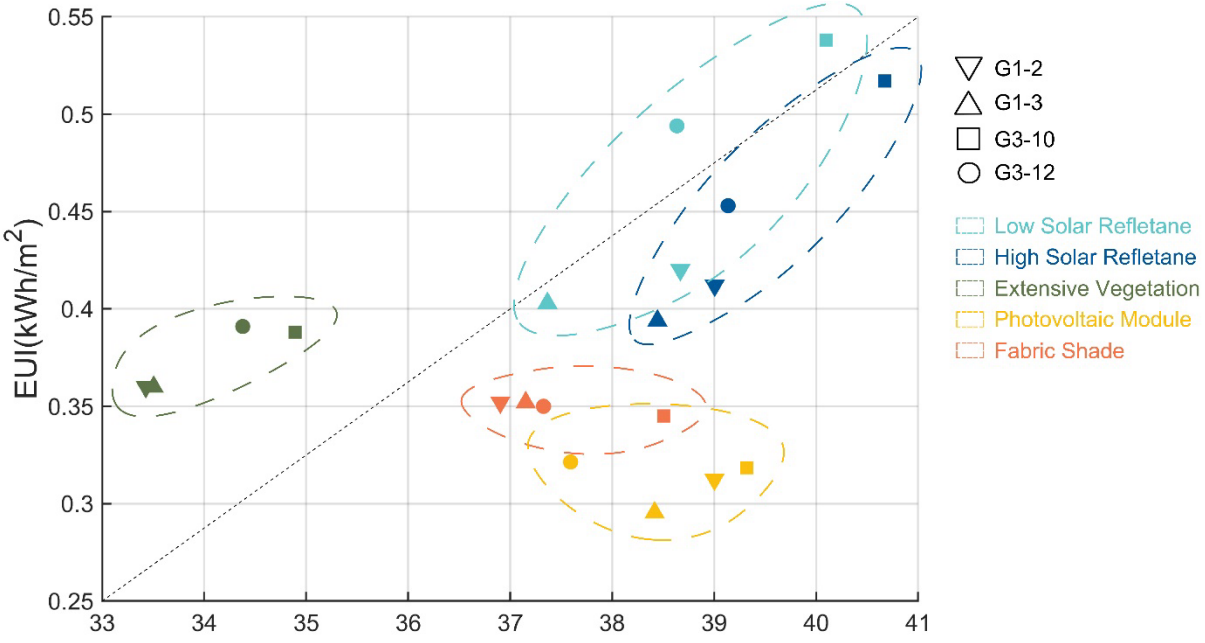

Fig. 15. Integrated performance of EUI and PET for different heat mitigation measures.

The results indicate that extensive vegetation measures are most effective in reducing courtyard PET, while photovoltaic module measures lean more towards decreasing building EUI. Fabric shade measures perform well in both reducing courtyard PET and building EUI. However, when only the solar reflectance ratio is altered, the excess heat merely shifts between outdoor and indoor environments, with the reduced outdoor PET translating into increased indoor energy consumption.

The extensive vegetation measure is the most effective in reducing outdoor T_{mrt} and PET among the localized heat measures. This is because a large amount of greenery can reduce the proportion of impervious surfaces, create shading, and carry away heat through evaporation, and many studies have concluded that increasing greenery is the best measure to optimize indoor and outdoor thermal environments and save energy [18, 37, 38]. However, the extensive vegetation measure also has drawbacks. In rural China, the open space in the courtyard is for connecting the wing rooms. Furthermore, some semi-manual agricultural work needs to be carried out in the open space in the courtyard. The extensive vegetation measure would invade the courtyard space and cause inconvenience, so this measure is not recommended in rural China, while the moderate vegetation measure is more suitable as a compromised alternative.

Photovoltaic module measures have the best energy savings. In scenarios with a low height-to-width ratio, it can provide shade for courtyards, effectively reducing T_{mrt} and PET, while converting solar energy hitting the rooftops into electrical energy. This not only lowers indoor T_o but also significantly reduces cooling energy consumption. While the photovoltaic module measure offers considerable benefits for the thermal environment and energy consumption, it also comes with drawbacks, such as issues related to light pollution or the ecological impacts on insects and birds.

By contrast, fabric shade measures offer a more balanced approach to optimizing indoor and outdoor environments and reducing energy consumption, without occupying additional space. Indeed, the study of horizontal shading components has become a focal point in recent years. Studies by Kristian et al. [39] demonstrated that textile sun shading in Italy, could reduce PET by 1°C. Research by Dalia et al. [40] in a school courtyard in Egypt, showed that textile shading devices covering 100% of the area could reduce T_{mrt} by over 20% and lower PET by more than 4°C. In addition, the fabric shade measure in Hangtou village is a removable facility, which uses fabric material with larger mesh in summer for shading and ventilation, and in winter it is replaced with polyvinyl chloride (PVC) material that is light transmitting but not wind transmitting, which can be used for warmth preservation.

Changing the solar reflectance of building surfaces does not have much effect on changing the outdoor thermal environment, and in the case of a village, the concrete wall with the lowest reflectance only reduces the T_{mrt} by about 3.0°C compared to the white wall with the highest reflectance. Salvati et al. [41] also found that the effect of changing the solar reflectance of building surfaces on changing the outdoor thermal environment in a London study is much smaller than that of solar reflectance of street surfaces. Mengrong et al. compared three scenarios of changing roof, wall, roof and wall solar reflectance in Guangzhou suburb, and the result was that only the scenario of changing wall solar reflectance had only 20% of the effect on the change of albedo. albedo change is only 20%, roof scenario 89%, and roof and wall scenario is as high as 139% [42].

More importantly, decreasing the solar reflectance of building surfaces increases indoor T_o and energy consumption, which means heavier economic pressure for rural areas in China, and this is not a good measure to improve the thermal environment and energy saving for rural areas.

4.2 Limitations

In this study, the measured data of R-2 and R-3 street spaces do not exactly overlap, which is different from

the results obtained from the simulations. It might be due to the location of street measurement points of R-2 and R-3 that are not exactly at the midpoint of the space in the actual measurements, where R-2 is close to the south side and R-3 is close to the north side, which is arranged because it cannot interfere with the passage of the street, and at the same time, there are clutter on the site that cannot be placed on the same side of the street. Such a difference leads to the fact that the SVF is not the same for the two street sites, which is considered as one of the main influencing factors of the outdoor space thermal environment [43, 44]. GUO et al. obtained the lowest surface temperatures when the SVF was in the middle of the range in the investigation of surface temperatures in Guangzhou City, and both too high and low SVFs lead to high surface temperatures [45].

The courtyard with a south wing has a lower T_{mrt} value compared to the courtyard with a south wall, which is evident in the solar reflectance measure and photovoltaic module measure for changing the surface of the material, but is largely ineffective in the extensive vegetation measure and fabric shade measure, or even the opposite. This situation is obvious under the solar reflectance and photovoltaic module measures, but has no effect under the extensive vegetation measure and fabric shade measure, or even the opposite effect. It is possible that the solar radiation on the surface of the courtyard enclosure is effectively reflected and the absorption of energy is reduced under the extensive vegetation and fabric shade measures [46].

5. Conclusion

This paper examined the effectiveness of the courtyard layout patterns and localized heat mitigation measures in reducing the rural heat island effect in centralized rural residences. The paper consists of three main parts. Firstly, the microclimate of three typical centralized residences and the countryside boundary is measured on site, which proves the existence of the rural heat island effect. Secondly, 22 types of courtyard layout patterns are simulated, and the effectiveness of the courtyard with a south wing in optimizing the thermal environment of rural centralized residences. Lastly, four types of localized heat mitigation measure in different layout patterns are simulated, and their effectiveness in relieving outdoor heat stress and saving energy is discussed.

Field measurements show that air temperatures in the outdoor spaces of centralized rural residences are 1.0°C higher compared to the village boundaries, that temperature maxima occur 2 hours later, and that thermal discomfort in centralized rural residences lasts up to 9 hours, 4 hours more than at the village boundaries.

The courtyard with a south wing significantly mitigates summer outdoor thermal stress compared to a south wall. It can reduce the maximum mean radiant temperature by up to 8%, shorten the duration of extreme thermal stress by 1.5 hours, and save daily energy usage intensity by 0.07 kWh/m^2.

Among the four localized heat mitigation measures, extensive vegetation and fabric shade measures stand out for alleviating outdoor thermal stress. Photovoltaic module measures excel in energy savings, whereas low solar reflectance measures increase energy consumption. Extensive vegetation measures can reduce the duration of extreme heat stress by 3 hours, and fabric shade measures by 2 hours. Photovoltaic modules could lower the daily EUI by 0.10-0.18 kWh/m^2. Low solar reflectance measures had negligible effect on mitigating outdoor thermal stress and could even increase the indoor operative temperature by 0.2°C - 0.5°C, leading to a rise in daily EUI by 0.01-0.04 kWh/m^2.

Therefore, this paper proposes to adopt courtyards with a south wing in newly built rural centralized residences, and promote the use of extensive vegetation measure and fabric shade to alleviate heat stress in summer, especially the fabric shade measure which can avoid occupying the space of courtyards and provide ventilation. Moreover, photovoltaic module measures should also be widely implemented. They can significantly reduce energy consumption while providing shading for courtyard spaces, effectively reducing outdoor thermal stress in these areas. This study explored the effectiveness of local measures in mitigating the

RHI effect, providing a basis for supporting managers and designers of centralized villages.

Acknowledgments

This research was supported by the 2023 Tianjin Philosophy and Social Science Planning Project (TJGLQN23-007).

Declaration of competing interest

The authors declare that they have no known competing financial interests or personal relationships that could have appeared to influence the work reported in this paper.

Appendix A. Instruments

Table A. 1
Parameters of field measurement instruments.

Measurement site	Instrument /Equipment	Measurement parameter	Interval	Accuracy
Street, courtyard, indoors	Temperature and relative humidity data logger /HOBO MX2301&MX1101	Air temperature	5min	0.01°C
		Relative humidity	5min	0.01%RH
Street, courtyard	Black-bulb thermometer /HQZY-1	Black globe temperature	5min	0. 1°C
	Multifunction Instrument / KIMO AMI310	Wind speed	1h	0.1m/s
	Fisheye lens /Sitger AK005	Fisheye photo	1d	
	Infrared thermal imager /FLUK Ti400	Surface temperature	3h	0.1°C
Village boundary square	Micro-meteorological station /PC-6	Air temperature	1min	0.1°C
		Relative humidity	1min	0.1%RH
		Wind speed	1min	0.1m/s
		Wind velocity	1min	1°
		Global radiation	1min	1W/m^2
		Direct radiation	1min	1 W/m^2

Appendix B. The simulation model settings

Table B. 1

Parameters of materials in ENVI-met simulation.

Facade materials						
Material	Application	Density (kg/m2)	Solar reflectance	Emissivity	Specific heat	Thermal conductivity
white Plaster	Wall Surface	1500	0.70	0.93	850	0.60
yellow Plaster	Wall Surface	1500	0.50	0.93	850	0.60
cement Plaster	Wall Surface	1700	0.30	0.93	1050	0.76
clear float glass	Clear Float Glass	2500	0.05	0.90	750	1.05
PE-black	Fabric Shade Nest	960	0.20	0.90	2100	0.40
Photovoltaic	Photovoltaic Module	5000	0.10	0.85	700	0.03
Tile	Roofing	1900	0.30	0.93	800	0.84
Soils materials						
Material	Application	Roughness(m)	Albedo	Emissivity		
Loamy soil	Courtyard	0.015	0.0	0.90		
Used Concrete	Street	0.01	0.25	0.90		
Vegetation						
Material	Application	Scale（m）	Albedo	Emissivity	Leaf type	Shortwave transmittance
Grass	Courtyard+Street	25（height）	0.20	0.97	Grass	0.30
Hedge light	N-S Street	2（height）	0.20	0.97	Deciduous	0.30
Small Palm	Courtyard+Street	5x3x3	0.18	0.96	Deciduous	0.30
Horse Chestnut	Courtyard	7.4x4.88x4.85	0.18	0.96	Deciduous	0.3

Table B. 2

ENVI-met parameters setting.

	Parameter	Value
Space	Location	Ju Xian
	Position	35.63 118.90
	Time zone	+8
	Model dimensions	L 167m* D 154m* H 30m L 149m* D 200m* H 20m
	Size of grid cell in meter	dx=1 dy=1 dz=1
Date & time	Start date	2023.07.31
	Start time	0:00
	Total simulation time	23h
Meteorology	Boundary conditions	Full forcing
	Forcing data	Wind Air temperature Clouds Humidity
	Measurement height	Air temperature & Relative humidity 1.2m Wind speed & direction 2m
	Roughness length	0.1m

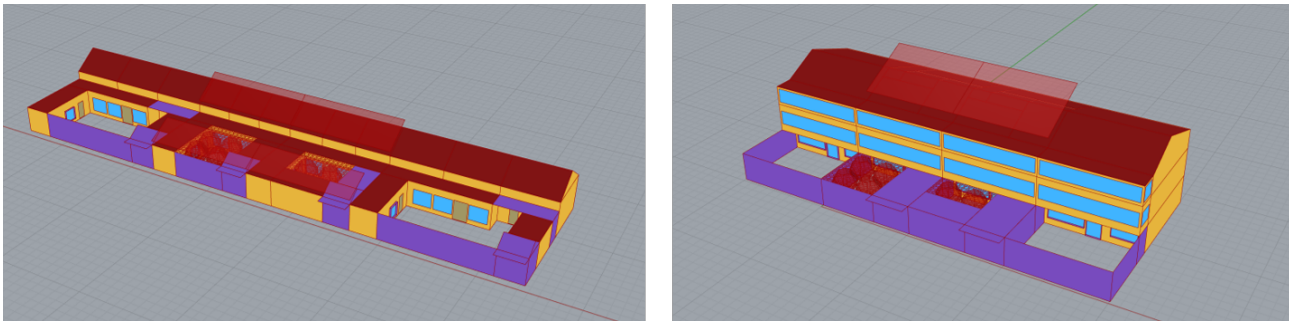

Fig.B. 1 LBT models of G1-2 and G1-3(right), G3-10 and G3-12(left).

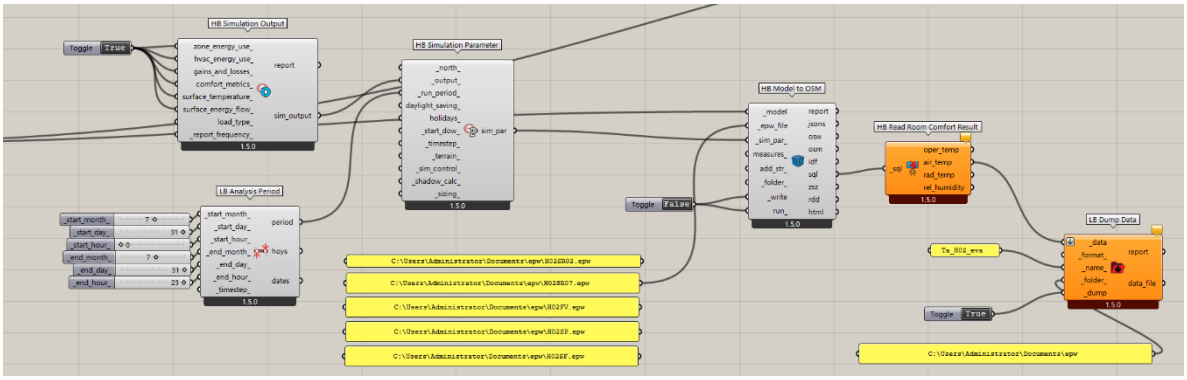

Fig.B. 2 LBT weather setting.

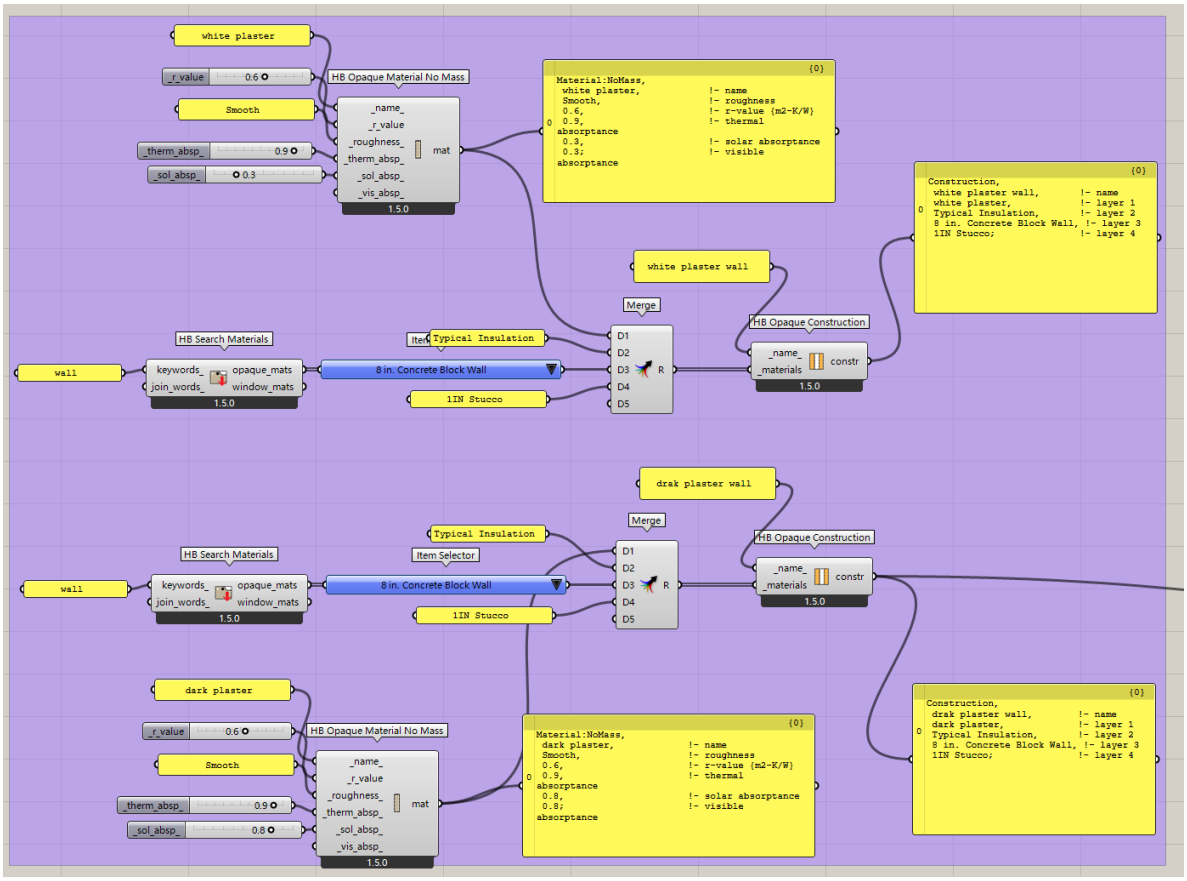

Fig.B. 3 Construction setting of LBT models' wall.

References

1.Liu, Z., M. H. Wang, Q. Q. Xiong and C. Liu (2020). "Does centralized residence promote the use of cleaner cooking fuels? Evidence from rural China." Energy Economics **91**.

2.Deilami, K., M. Kamruzzaman and Y. Liu (2018). "Urban heat island effect: A systematic review of spatio-temporal factors, data, methods, and mitigation measures." International Journal of Applied Earth Observation and Geoinformation **67**: 30-42.

3.Rajagopal, P., R. S. Priya and R. Senthil (2023). "A review of recent developments in the impact of environmental measures on urban heat island." Sustainable Cities and Society **88**.

4.Shen, Z., J. Shi, J. Tan and H. Yang (2020). "The Migration of the Warming Center and Urban Heat Island Effect in Shanghai During Urbanization." Frontiers in Earth Science **8**.

5.Chen, M., Y. Zhou, M. Hu and Y. Zhou (2020). "Influence of Urban Scale and Urban Expansion on the Urban Heat Island Effect in Metropolitan Areas: Case Study of Beijing–Tianjin–Hebei Urban Agglomeration." Remote Sensing **12**(21): 3491.

6.Wang, Z. H. (2022). "Reconceptualizing urban heat island: Beyond the urban-rural dichotomy." Sustainable Cities and Society **77**.

7.Guo, G. H., Z. F. Wu, Z. Cao, S. Y. Li and Y. B. Chen (2023). "Assessment of spatio-temporal intra-rural heat island variability based on IoT monitoring." Urban Climate **52**.

8.Lai, D. Y., W. Y. Liu, T. T. Gan, K. X. Liu and Q. Y. Chen (2019). "A review of mitigating strategies to improve the thermal environment and thermal comfort in urban outdoor spaces." Science of the Total Environment **661**: 337-353.

9.Lau, K. K. L., C. Ren, J. Ho and E. Ng (2016). "Numerical modelling of mean radiant temperature in high-density sub-tropical urban environment." Energy and Buildings **114**: 80-86.

10.Qin, Y. H. (2015). "Urban canyon albedo and its implication on the use of reflective cool pavements." Energy and Buildings **96**: 86-94.

11.Yang, X. Y. and Y. G. Li (2015). "The impact of building density and building height heterogeneity on average urban albedo and street surface temperature." Building and Environment **90**: 146-156.

12.Tian, L., Y. Li, J. Lu and J. Wang (2021). "Review on Urban Heat Island in China: Methods, Its Impact on Buildings Energy Demand and Mitigation Strategies." Sustainability **13**(2).

13.Ghaffarianhoseini, A., U. Berardi and A. Ghaffarianhoseini (2015). "Thermal performance characteristics of unshaded courtyards in hot and humid climates." Building and Environment **87**: 154-168.

14.Taleghani, M., L. Kleerekoper, M. Tenpierik and A. van den Dobbelsteen (2015). "Outdoor thermal comfort within five different urban forms in the Netherlands." Building and Environment **83**: 65-78.

15.Letizia, M., M. Letizia, M. Andreas and M. Andreas (2017). "Influence of height/width proportions on the thermal comfort of courtyard typology for Italian climate zones." Sustainable Cities and Society.

16.Taha, H. S., D.J. Akbari, H. (1992). High-Albedo Materials for Reducing Building Cooling Energy Use. Lawrence Berkeley National Laboratory. H. Taha, Sailor, D., & Akbari, H. .

17.Salvati, A., M. Kolokotroni, A. Kotopouleas, R. Watkins, R. Giridharan and M. Nikolopoulou (2022). "Impact of reflective materials on urban canyon albedo, outdoor and indoor microclimates." Building and Environment **207**.

18.Tsoka, S., A. Tsikaloudaki and T. Theodosiou (2018). "Analyzing the ENVI-met microclimate model's performance and assessing cool materials and urban vegetation applications-A review." Sustainable Cities and

Society **43**: 55-76.

19.Buyantuyev, A. and J. G. Wu (2010). "Urban heat islands and landscape heterogeneity: linking spatiotemporal variations in surface temperatures to land-cover and socioeconomic patterns." Landscape Ecology **25**(1): 17-33.

20.Chen, A. L., X. A. Yao, R. H. Sun and L. D. Chen (2014). "Effect of urban green patterns on surface urban cool islands and its seasonal variations." Urban Forestry & Urban Greening **13**(4): 646-654.

21.Shashua-Bar, L. and M. E. Hoffman (2004). "Quantitative evaluation of passive cooling of the UCL microclimate in hot regions in summer, case study: urban streets and courtyards with trees." Building and Environment **39**(9): 1087-1099.

22.Zheng, R. F., Y. F. Zheng, L. Cong, J. H. Choi and H. Jung (2020). "Climate Adaptive Design Improvement Strategies of Traditional Dwellings in Southern Zhejiang for the Plum Rain Season Considering Comfort Conditions." Energies **13**(6): 20.

23.Juan Angel, A., A. A. Juan, A. R. Lea, R. Lea, J. Y. K. Elliot, J. Y. K. Elliot, T. Yon Sun, T. Yon Sun, K. N. Leslie and K. N. Leslie (2022). "Measuring and comparing thermal comfort in outdoor and semi-outdoor spaces in tropical Singapore." Urban Climate.

24.Kántor, N., L. Chen and C. V. Gál (2018). "Human-biometeorological significance of shading in urban public spaces—Summertime measurements in Pécs, Hungary." Landscape and Urban Planning **170**: 241-255.

25.Elena, G. N., G.-N. Elena, G.-N. Elena, B. Benoît, B. Benoit, R. Helena Coch, R. Helena Coch and C. Helena (2020). "Assessing the cooling effect of urban textile shading devices through time-lapse thermography." Sustainable Cities and Society.

26.Liu, Z., Z. J. Zhou and C. Liu (2023). "Estimating the impact of rural centralized residence policy interventions on energy poverty in China." Renewable & Sustainable Energy Reviews **187**.

27.Rao, X. X., J. D. Zhou, K. L. Ding, J. F. Wang, J. Q. Fu and Q. H. Zhu (2022). "Research on the Cultural Tracing of the Patriarchal Clan System of Traditional Buildings in the Eastern Zhejiang Province, China, Based on Space Syntax: The Case Study of Huzhai in Shaoxing." Sustainability **14**(12).

28.Salata, F., L. Golasi, R. D. Volloaro and A. D. Vollaro (2016). "Urban microclimate and outdoor thermal comfort. A proper procedure to fit ENVI-met simulation outputs to experimental data." Sustainable Cities and Society **26**: 318-343.

29.Yang, X., L. Zhao, M. Bruse and Q. Meng (2013). "Evaluation of a microclimate model for predicting the thermal behavior of different ground surfaces." Building and Environment **60**: 93-104.

30.Li, M. L., Y. Y. Jin and J. L. Guo (2022). "Dynamic characteristics and adaptive design methods of enclosed courtyard: A case study of a single-story courtyard dwelling in China." Building and Environment **223**.

31.Han, T., Q. Huang, A. X. Zhang and Q. Zhang (2018). "Simulation-Based Decision Support Tools in the Early Design Stages of a Green Building-A Review." Sustainability **10**(10).

32.Zhang, A. X., R. Bokel, A. van den Dobbelsteen, Y. C. Sun, Q. Huang and Q. Zhang (2017). "An integrated school and schoolyard design method for summer thermal comfort and energy efficiency in Northern China." Building and Environment **124**: 369-387.

33.Matzarakis, A., F. Rutz and H. Mayer (2007). "Modelling radiation fluxes in simple and complex environments - application of the RayMan model." International Journal of Biometeorology **51**(4): 323-334.

34.Shashua-Bar, L., O. Potchter, A. Bitan, D. Boltansky and Y. Yaakov (2010). "Microclimate modelling of street tree species effects within the varied urban morphology in the Mediterranean city of Tel Aviv, Israel." International Journal of Climatology **30**(1): 44-57.

35.Groleau, D. and P. G. Mestayer (2013). "Urban Morphology Influence on Urban Albedo: A Revisit with the SOLENE Model." Boundary-Layer Meteorology **147**(2): 301-327.

36.Morini, E., B. Castellani, A. Presciutti, E. Anderini, M. Filipponi, A. Nicolini and F. Rossi (2017). "Experimental Analysis of the Effect of Geometry and Facade Materials on Urban District's Equivalent Albedo." Sustainability **9**(7): 12.

37.Balany, F., A. W. M. Ng, N. Muttil, S. Muthukumaran and M. S. Wong (2020). "Green Infrastructure as an Urban Heat Island Mitigation Strategy-A Review." Water **12**(12): 22.

38.Darvish, A., G. Eghbali and S. R. Eghbali (2021). "Tree-configuration and species effects on the indoor and outdoor thermal condition and energy performance of courtyard buildings." Urban Climate **37**: 26.

39.Kristian, F., A. Ernesto and M. Lia (2023). "Sun-Shading Sails in Courtyards: An Italian Case Study with RayMan." Sustainability.

40.Dalia, E., E. L. G. Dalia, E. Sara and E. Sara (2021). "The impact of sun sail-shading strategy on the thermal comfort in school courtyards." Building and Environment.

41.Salvati, A., M. Kolokotroni, A. Kotopouleas, R. Watkins, R. Giridharan and M. Nikolopoulou (2022). "Impact of reflective materials on urban canyon albedo, outdoor and indoor microclimates." Building and Environment **207**: 16.

42.Mengrong, L., Z. Liyue, L. Qingman, H. Jian, H. Jiajia, W. Xuemei and W. Weiwen (2023). "Quantifying cooling benefits of cool roofs and walls applied in building clusters by scaled outdoor experiments."

43.Jamei, E., P. Rajagopalan, M. Seyedmahmoudian and Y. Jamei (2016). "Review on the impact of urban geometry and pedestrian level greening on outdoor thermal comfort." Renewable & Sustainable Energy Reviews **54**: 1002-1017.

44.He, X. C., W. J. Gao and R. Wang (2021). "Impact of urban morphology on the microclimate around elementary schools: A case study from Japan." Building and Environment **206**: 14.

45.Guo, G. H., X. Q. Zhou, Z. F. Wu, R. B. Xiao and Y. B. Chen (2016). "Characterizing the impact of urban morphology heterogeneity on land surface temperature in Guangzhou, China." Environmental Modelling & Software **84**: 427-439.

46.Diz-Mellado, E., V. P. Lopez-Cabeza, J. Roa-Fernandez, C. Rivera-Gomez and C. Galan-Marin (2023). "Energy-saving and thermal comfort potential of vernacular urban block porosity shading." Sustainable Cities and Society **89**: 17.